Mon. Not. R. Astron. Soc. **000**, 000–000 (1999)

Surface motion in the pulsating DA white dwarf G 29-38

M. H. van Kerkwijk[1,2,3], J. C. Clemens[1,4] and Y. Wu[5,6]
[1] *Palomar Observatory, California Institute of Technology 105-24, Pasadena, CA 91125, USA*
[2] *Institute of Astronomy, University of Cambridge, Madingley Rd, Cambridge, CB3 0HA, UK*
[3] *Astronomical Institute, Utrecht University, P.O. Box 80000, 3508 TA Utrecht, The Netherlands; M.H.vanKerkwijk@astro.uu.nl*
[4] *Department of Physics and Astronomy, University of North Carolina, Chapel Hill, NC 27599-3255, USA; clemens@physics.unc.edu*
[5] *Theoretical Astrophysics, California Institute of Technology 130-33, Pasadena, CA 91125, USA*
[6] *Astronomy Unit, School of Math. Sci., Queen Mary and Westfield College, Mile End Road, London E1 4NS, UK; Y.Wu@qmw.ac.uk*

12 November 1999

ABSTRACT
We present time-resolved spectrophotometry of the pulsating DA white dwarf G 29-38. As in previous broad-band photometry, the light curve shows the presence of a large number of periodicities. Many of these are combination frequencies, i.e., periodicities occurring at frequencies that are sums or differences of frequencies of stronger, real modes. We identify at least six real modes, and at least five combination frequencies. We measure line-of-sight velocities for our spectra and detect periodic variations at the frequencies of five of the six real modes, with amplitudes of up to $5\,\mathrm{km\,s^{-1}}$. We argue that these variations reflect the horizontal surface motion associated with the g-mode pulsations. No velocity signals are detected at any of the combination frequencies, confirming that the flux variations at these frequencies do not reflect physical pulsation, but rather mixing of frequencies due to a non-linear transformation in the outer layers of the star. We discuss the amplitude ratios and phase differences found for the velocity and light variations, as well as those found for the real modes and their combination frequencies, both in a model-independent way and in the context of models based on the convective-driving mechanism. In a companion paper, we use the wavelength dependence of the amplitudes of the modes to infer their spherical degree.

Key words: stars: individual (G 29-38) – stars: oscillations – white dwarfs

1 INTRODUCTION

Pulsating white dwarfs show brightness variations at a range of frequencies, with amplitudes of up to a few per cent. They appear to be normal white dwarfs, except for the fact that they lie in a special temperature range, or instability strip, in which they are unstable to pulsations. There are instability strips for all three of the main white dwarf types, DA, DB and DO (atmosphere dominated by H I, He I and He II, respectively), around 12 000, 23 000 and 100 000 K, respectively.

Pulsating white dwarfs offer the prospect of physical insight via a number of different methods. One is asteroseismology, the determination of a white dwarf's internal structure through the comparison of observed periodicities with model predictions of stellar eigen-modes. Another method analyses which modes are present, what their amplitudes are and how the amplitudes vary. The aim is to learn about the physics of the upper layers of the star, by determining the way in which modes interact with different parts of the star and with each other.

Robinson, Kepler & Nather (1982) showed that white dwarfs pulsate in non-radial gravity modes, and that the observed brightness variations result from perturbations of their temperature, not of their geometry or gravity. They also estimated the expected variations in the line-of-sight velocity and the line profile, and concluded that these would be too small to measure with then available instrumentation. As we will show below, this statement no longer holds.

The pulsations were originally thought to be excited in an ionisation zone, as in classical pulsators such as the Cepheids. The dynamics in DA and DB pulsating white dwarfs are rather unlike those in classical pulsators, however, in that for the white dwarfs the surface convection zone can respond almost instantaneously to gravity-mode pulsations, because the turnover times are much shorter than the mode periods. In a series of papers, Brickhill (1983, 1990, 1991a,b) has described the response in detail, and concludes it leads to significant "convective driving", which will be sufficient to overcome the damping in the radiative interior for modes with periods of order of or shorter than the thermal response time of the convection zone. Brickhill's partly numerical results have recently been confirmed analytically (Wu 1997; Goldreich & Wu 1999a).

The DA and DB pulsating white dwarfs often show power at frequencies that are the sums or differences of frequencies with stronger power. Based on the density of the theoretical gravity-mode spectra in the relevant frequency range, it has been argued that these "combination frequencies" do not represent real eigen-modes, but are instead produced by nonlinear mixing of pulsation signals of real eigen-modes ("parent modes") in the outer layer of the star. Some support for this idea comes from observed correlations in power.

Brickhill (1992a,b) has suggested that the mixing is a by-product of the interaction between the pulsations and the convection zone. Because of the relatively slow thermal response of the convection zone, flux variations take some time to appear at the surface, and they are reduced in amplitude. But the thickness of the convection zone is modulated by the pulsation, so that the signal is not only diminished and delayed, but also distorted. It is the latter distortion which translates into the power seen at combination frequencies.

Both to be able to make an asteroseismological analysis and to verify the pulsation models, it is essential to identify periodicities with eigen-modes, i.e., obtain their radial order n, spherical degree ℓ and azimuthal order m. For some DB and DO variables, it has been possible to obtain reasonably sound identifications from a direct comparison of observed frequencies with model predictions. However, for many other stars, including all DA variables, there are either too few modes, or the mode structure is too variable.

Robinson et al. (1995) implemented a method to identify spherical degree ℓ, which combined broad-band measurements of mode amplitudes at optical and UV wavelengths. It makes use of the wavelength dependence of limb darkening, which causes the pulsation amplitudes to vary with wavelength in a manner that depends on ℓ. Based on its success, we were motivated to implement a variation of this method which uses high signal-to-noise time-resolved spectrophotometry at optical wavelengths only. As will become clear, our initial data on the star G 29-38 showed variations not only in flux but also in line-of-sight velocity. The broadened scope, as well as the increased complexity in modeling the flux variation as a function of wavelength, made us decide to present the amplitudes and phases of the modes as a function of wavelength in a separate paper* (Clemens et al. 1998, hereafter Paper II).

In this paper, we focus on the implications of the line-of-sight velocity variations. We first briefly review the basic properties of G 29-38 (Section 2), and then describe the observation and data reduction in detail (Section 3). In Section 4, we analyse the periodicities in the light curve, and in Section 5 we search for corresponding variations in the line-of-sight velocity curve. We discuss the implications of our results in Section 6, both in a model-independent way and in the context of the convective driving models described above.

* We are far from having exhausted the information in our data; we will gladly make it available in digital form to anyone interested in analyzing it further.

2 G 29-38

G 29-38 (ZZ Psc; WD 2326+029) was discovered as a variable by Shulov & Kopatskaya (1974) and studied in some detail by McGraw and Robinson (1975). It is bright ($V \simeq 13.0$), at the cool end of the instability strip ($T = 11800$ K, Bergeron et al. 1995; cf. Paper II) and shows large-amplitude modulations (up to a few per cent). The source remained relatively obscure until Zuckerman & Becklin (1987) reported an infrared excess, which is still unexplained (for recent developments, see Kleinman et al. 1994; Koester, Provencal & Shipman 1997). In 1987, it was first subjected to scrutiny with the Whole Earth Telescope (WET; Winget et al. 1990). Unlike for the variable DBs and DOs, however, the observations – while of excellent quality – yielded more questions than answers. Partly, this is because of the complex and variable frequency spectrum of G 29-38: typically, dozens of periodicities are seen, with many occurring at frequencies that are differences or sums of the frequencies of other periodicities.

Kleinman et al. (1998) discussed an extensive collection of data sets, obtained over many seasons. They find that many periodicities are variable and unstable from year to year, but some do recur. By considering the whole ensemble, they could identify with some certainty which periodicities were associated with real modes and which with combination frequencies. They found nineteen real modes, the majority of which very likely have $\ell = 1$. However, due to the vagaries of the mode characteristics – especially the enigmatic, confusing behavior of multiplets, showing different and changing splitting – their results are suggestive, but not definitive.

3 OBSERVATIONS

Spectra of G 29-38 were taken on 1996 November 19 using the Low Resolution Imaging Spectrometer (Oke et al. 1995) on the 10-m Keck II telescope. From 4:42 till 9:25 UT, a continuous series of 700 12 s exposures was made. Only 100 pixels in the spatial direction (corresponding to 21.5 arcsec), binned by a factor 2, were read out through two amplifiers, leading to a read-out and re-set time in between exposures of about 12 s. The 600 line mm^{-1} grating was used, covering the range 3450–5950 Å at 1.2 Å pix^{-1}. The weather started photometric, and we used a 8.7 arcsec slit to make use of that. Hence, the seeing of 1.2 arcsec determined the wavelength resolution of ~ 7 Å. In principle, it would have been best to keep the slit at the parallactic angle in order for refraction not to influence the wavelength scale, but this would have required non-standard guiding and we decided to keep the slit at position angle 0 instead.

At the end of the series, a bank of cloudlets came in, causing the last 55 spectra, as well as one spectrum some ten minutes earlier, to have a reduced source and increased sky rate (the moon was up, so these are easy to identify). We have not used any of these spectra in our analysis.

The series of exposures was followed by fifteen 4 s integrations on the spectrophotometric flux standard G 191-B2B, using the same setup. Each of the series was followed by Hg/Kr wavelength calibration and halogen flat-field frames.

The reduction of all spectra was done as follows. The frames were bias-corrected separately for the two amplifiers using the overscan regions, and then corrected for the gain difference between the two amplifiers as determined from halogen spectra. The sky background was estimated by fitting parabolae for each position in the dispersion direction, excluding 21 binned pixels (~ 9) centred on the stellar spectrum. The latter pixels were used to estimate the stellar flux using an optimal weighting scheme similar to that of Horne (1986). Note that we did not flat-field the data. The reason is that we had been unable, due to an instrument failure shortly after taking the exposures on G191-B2B, to obtain a large enough number of halogen spectra to construct a flat-field that matched the signal-to-noise ratio of our observations, especially in the blue. Since the flat fields that we did have appeared very smooth, we decided to forego flat-fielding altogether. The resulting spectra look smooth (Fig. 1), except for a few pixels that are easy to identify. Note the presence of metals – Ca II λ3933 and Mg II λ4481 – uncovered only recently by Koester et al. (1997).

Accurate flux calibration was not possible, since the G 191-B2B spectra were taken while the bank of cloudlets was still passing. We selected the three most exposed spectra of the series of fifteen acquired, as these have comparable count rates and hence may not be influenced too much, making the relative flux calibration more reliable[†]. From these three, we derived the instrumental response using the model fluxes provided by Bohlin, Colina & Finley (1995), and the atmospheric extinction curve of Beland, Boulade & Davidge (1988). Typical examples of relatively high and low-flux spectra, as well as the average spectrum, are shown in Fig. 1.

Special care was taken to correct the wavelength scale for instrumental effects due to flexure and atmospheric refraction. Both effects can be seen in the pixel positions on the detector as a function of time of the O I λ5577 sky line and the Balmer lines (Fig. 2a). Here, the positions were derived by cross-correlation of the spectra with the average of those spectra taken with the slit position angle less than 20 away from the parallactic angle. The break at $t - \bar{t} \simeq 2000$ s in the Balmer-line positions is due to guiding being stopped and re-started (to take a guider image).

The flexure is described well by a cubic fit to the sky-line positions. After correction for the flexure, as well as for the jump due to switching the guider off and on, the positions of the Balmer lines vary linearly with what is expected from refraction ($\sin\alpha \tan\zeta$, where α is the difference between parallactic and position angle, and ζ the zenith distance). The different slopes indicate that our guiding wavelength was approximately 7000 Å, as expected for the CCD camera used. We used this value to calculate the wavelength corrections for the whole spectrum.

Since our spectra were taken through a wide slit, small movements of the star will result in random apparent wavelength shifts for individual spectra. The effect can be estimated by measuring the shifts along the slit from the spatial profiles (averaged over some number of pixels along the dispersion direction). We find a root-mean-square variation in these of 0.084 binned pixels, corresponding to 0036. Assuming the variations in the dispersion direction are similar, one thus expects variations of about 0.2 Å, or 14 km s^{-1} at Hγ.

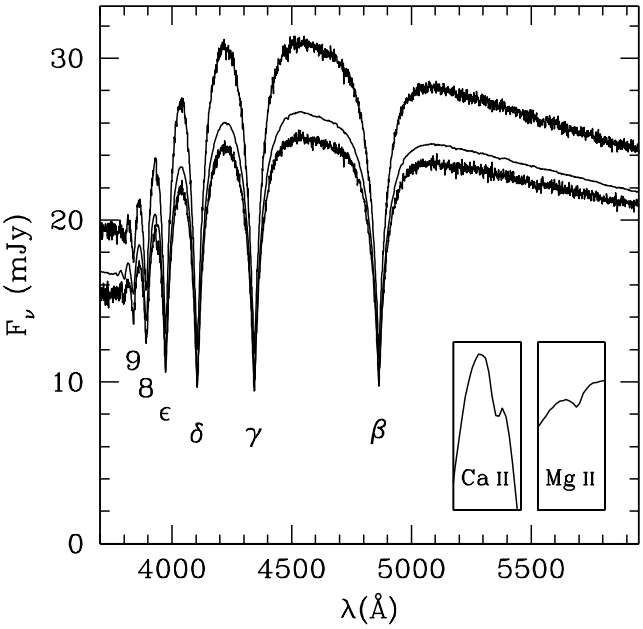

Figure 1. Average of all spectra and examples of spectra taken at times of high and low flux (times -7444 and -7080 s in Fig. 2b). Apart from the Balmer lines (marked), weak lines due to Ca II λ3933 and Mg II λ4481 are also present (see insets; size 40 Å by 2 mJy). The other irregularities in the average spectrum are due to pixel-to-pixel sensitivity variations (see text).

Apparent brightness variations can result from varying slit losses due to seeing-related changes in the width of the stellar images. From the spatial profiles, we find 10% root-mean-square variations around the average full width at half maximum of 3 binned pixels (12). Using images taken with LRIS for other projects, we estimate that the slit losses with an 87×90 aperture are about 1% on average. Assuming that the slit losses scale approximately quadratically with the seeing, one thus expects apparent brightness variations of the order of 0.2%. This is smaller than the Poisson noise in individual wavelength elements, but dominates in the average light curve discussed below. It is also much larger than variations due to scintillation ($\sim$0.012%; Young 1967).

4 PERIODICITIES

In Fig. 2b, we show the continuum light curve, constructed by averaging the 5200–5500 Å region. The light curve shows the presence of a number of periodicities, and is similar to light curves observed before (see Section 2). The Fourier transform is shown in Fig. 3a. Most of the power is at frequencies below 6 mHz. An idea of the background level can be obtained from the 10–20 mHz region (see inset in figure), where little evidence for any periodicity is seen. In this region, we find a root-mean-square amplitude of about 0.025%. The corresponding root-mean-square variation is half that, and one infers root-mean-square variations in the fluxes of about $\frac{1}{2}\sqrt{N_{\rm data}} \times 0.025\% = 0.32\%$ (where $N_{\rm data} = 644$ is

[†] Perhaps surprisingly, our estimated flux in the average spectrum compares quite well with the observed V magnitude of 13.05 ± 0.05 (22 ± 1 mJy; McCook & Sion 1987).

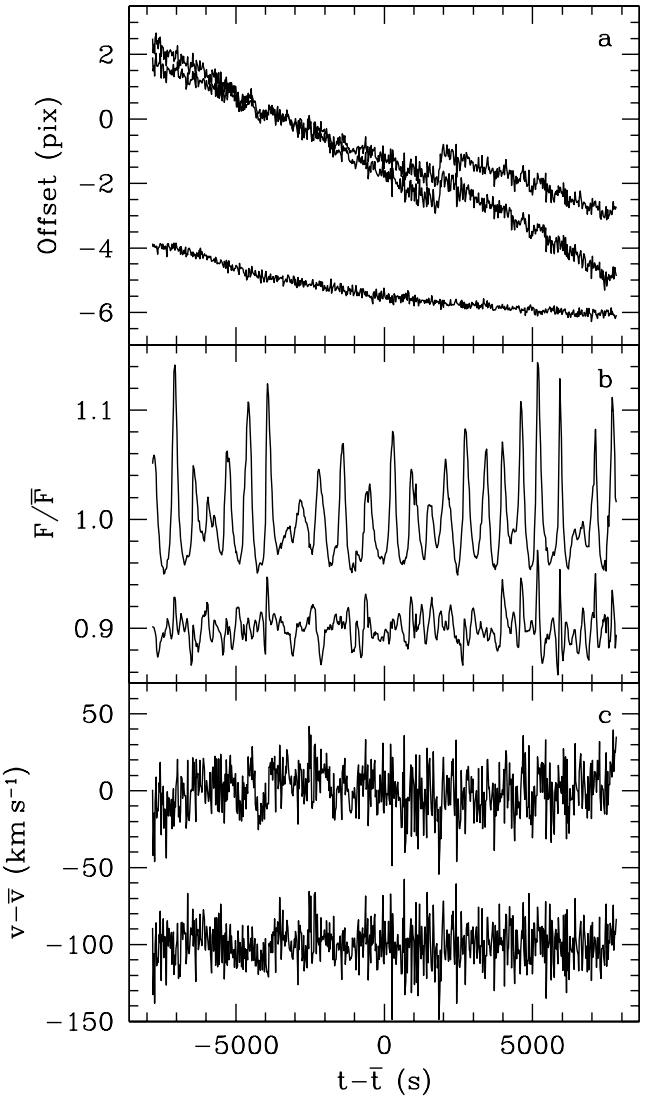

Figure 2. (a) Variations as a function of time in the pixel position on the detector of the O I λ5577 sky line (bottom curve; offset by -5 pixels), Hβ (top curve at right) and Hϵ (middle curve at right). The smooth variations are due to flexure in the spectrograph and differential refraction in the atmosphere. (b) Fractional brightness variation (top curve) in the line-free wavelength region 5200–5500 Å, and residual variation (bottom curve, offset by 0.9) remaining after taking out the eleven periodic variations with amplitudes larger than 0.55% and a constant term (Fig. 3a; Table 1). (c) Line-of-sight velocity variations determined from fits to the Hβ, Hγ and Hδ lines (top curve), and the residuals (bottom curve, offset by $-100\,\mathrm{km\,s^{-1}}$) remaining after taking out variation at the eleven periods present in the light curve, as well as a cubic term.

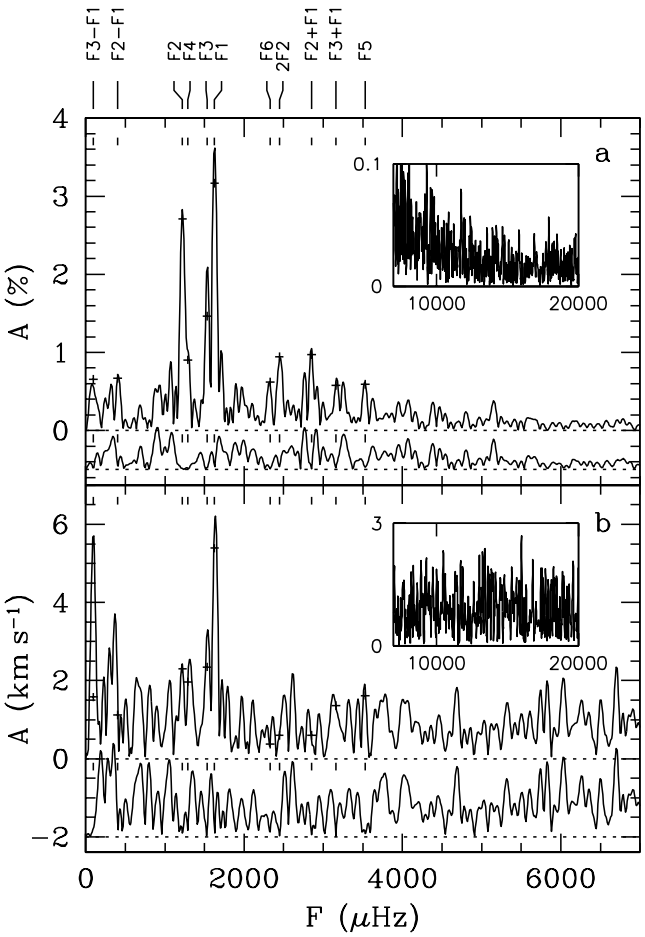

Figure 3. Fourier transform of the light curve (a) and line-of-sight velocity curve (b). The eleven strongest peaks in the Fourier transform of the light curve are indicated and labeled. The pluses indicate the amplitudes derived from fitting eleven cosine waves (plus a constant for the light curve and a cubic term for the radial-velocity curve). The bottom curve in each panel shows the Fourier transform of the residuals, offset from zero for clarity. The insets show the Fourier transform at higher frequencies.

the number of data points), more or less consistent with the estimate made above based on varying slit losses. We believe essentially all the signal seen in the main panel of Fig. 3a, which is well above 0.025%, reflects stellar variability.

We identified the periodicities sequentially. We started by measuring the approximate frequency of the highest peak and fitting the data to a function of the form $C + A\cos(2\pi f t' - \phi)$, where $t' = t - 6{:}52{:}08$ UT is the time relative to the mid-observing time, solving for pulsation frequency f, phase ϕ and amplitude A, plus a constant offset C. Next, we identify the highest remaining peak in the Fourier transform of the residuals and include another cosine wave in the fit, etc. For combination frequencies, we held the frequencies fixed at the corresponding combinations of parent-mode frequencies. The decision whether a peak corresponded to a combination frequency or to a real mode, was generally made consulting the work of Kleinman (1995); in all cases, the amplitude of the combination frequency was the smallest of the peaks involved. Continuing as long as the next largest peak had not been influenced greatly by removing the previous

Table 1. Strong Pulsation Frequencies in G 29-38

Real mode	P (s)	f (μHz)	$A_{\rm L}$ (%)	$\Phi_{\rm L}$ ()	$A_{\rm V}$ (km s^{-1})	$\Phi_{\rm V}$ ()	$R_{\rm V}$	$\Delta\Phi_{\rm V}$ ()
F1	614	1628.0 ± 0.9	$3.17 \pm .08$	-168 ± 2	5.4 ± 0.8	-116 ± 8	17 ± 3	52 ± 8
F2	818	1223.0 ± 0.9	$2.71 \pm .08$	132 ± 2	2.3 ± 0.8	176 ± 19	11 ± 4	44 ± 19
F3	653	1531.2 ± 1.8	$1.46 \pm .08$	36 ± 3	2.4 ± 0.8	59 ± 19	17 ± 6	23 ± 19
F4	776	1288.7 ± 3.9	$0.90 \pm .08$	40 ± 6	2.0 ± 0.8	50 ± 22	27 ± 11	10 ± 23
F5	283	3528.8 ± 4.9	$0.59 \pm .08$	55 ± 8	1.6 ± 0.8	131 ± 27	12 ± 6	76 ± 28
F6	430	2327.6 ± 4.9	$0.62 \pm .08$	-86 ± 8	0.4 ± 0.8	···	4 ± 9	···
Combination frequency	P (s)	f (μHz)	$A_{\rm L}$ (%)	$\Phi_{\rm L}$ ()	$A_{\rm V}$ (km s^{-1})	$\Phi_{\rm V}$ ()	$R_{\rm C}$	$\Delta\Phi_{\rm C}$ ()
F2 + F1	351	2851.1	$0.97 \pm .08$	-33 ± 5	0.6 ± 0.8	···	5.7 ± 0.5	3 ± 5
F2 − F1	2469	405.0	$0.67 \pm .08$	34 ± 7	1.1 ± 0.8	···	3.9 ± 0.5	-26 ± 7
2F2	409	2446.1	$0.95 \pm .08$	-131 ± 5	0.6 ± 0.8	···	12.9 ± 1.4	-35 ± 7
F3 + F1	317	3159.2	$0.58 \pm .08$	-129 ± 8	1.4 ± 0.8	···	6.2 ± 1.0	3 ± 9
F3 − F1	10323	96.9	$0.66 \pm .09$	159 ± 7	1.6 ± 1.1	···	7.1 ± 1.0	3 ± 8

Notes. For the real modes, $R_{\rm V} = (A_{\rm V}/2\pi f)/A_{\rm L}$ in units of 10 km rad^{-1} %$^{-1}$ and $\Delta\Phi_{\rm V} = \Phi_{\rm V} - \Phi_{\rm L}$. For the combination frequencies, $f = f^i \pm f^j$, with for difference frequencies i and j chosen such that f is positive, $R_{\rm C} = A_{\rm L}^{i\pm j}/n_{ij}A_{\rm L}^i A_{\rm L}^j$ (with n_{ij} the number of possible permutations of i and j; unity for $i = j$, 2 otherwise) and $\Delta\Phi_{\rm C} = \Phi_{\rm L}^{i\pm j} - (\Phi_{\rm L}^i \pm \Phi_{\rm L}^j)$. The uncertainties in the parameters for the light curve should be seen as indicating relative uncertainties only, as the light curve is not described well by the eleven modes fitted and the deviations from the fit are definitely not distributed normally (see text and Fig. 2b). The estimates given here were obtained by multiplying the observational errors by such a factor that $\chi^2_{\rm red} = 1$. For the velocity curve, the estimates of the uncertainties should be reliable. The uncertainty distributions on amplitude and phase are not normal, but those on $A\cos\Phi$ and $A\sin\Phi$ are (see Section 5.1).

peaks, we found eleven periodicities with amplitudes larger than 0.55%.

Of the eleven periodicities found, there appear to be six real and five combination frequencies. These are listed in Table 1 and the corresponding peaks are identified in Fig. 3a. Comparing our periodicities with those found by Kleinman (1995), we find that most periodicities have been seen before. The exceptions are: (i) F6: power at 430 s has only been seen as an apparent harmonic of a strong 860 s mode; (ii) F3+F1: power at F1 (614 s) and F3 (653 s) has not been seen simultaneously before, and hence neither has this combination (although power at 317 s due to a different combination has been observed); and (iii) F2−F1 and F3−F1: at 2469 and 10322 s, these periods are longer than any generally considered (the identification of F3−F1 should be considered tentative here too). Absent is power at 400 s, which has been present in almost all observations so far.

From the residuals, it is clear that the eleven modes do not account well for the observed light curve (with our estimate of 0.2% root-mean-square uncertainties, we find a formal $\chi^2_{\rm red} \simeq 50$). We have tried continuing the identification process (see appendix), but fail to account for all the variability. Therefore, we decided to focus on the eleven modes for which we have full confidence. We note, however, that because of the additional power and the resulting non-normal deviations, the formal errors on the parameters are not very meaningful. To get an idea of relative uncertainties, we have scaled up the errors on the data points such that the reduced χ^2 equals unity.

A puzzling aspect of our results is that the three largest periodicities appear to have frequencies related to each other by simple integer ratios: $f_2 : f_1 \simeq 3 : 4$, $f_2 : f_3 \simeq 4 : 5$. Both are correct to within 0.2%. After identifying more modes and including these in the fit (see appendix), the ratios become more accurate (to within 0.1%). Furthermore, another mode, F8, is identified for which $f_8 : f_1 \simeq 2 : 3$, again to within 0.1%. Similar close coincidences have not been found in the observations of Kleinman (1995) and it may be that they are in some way due to our relatively short time span, perhaps in combination with the badness of the fit, especially near the light maxima (see Fig. 2b). On the other hand, these ratios may represent unexplored physics underlying the pulsation spectrum. For the present time, we will ignore possible complications arising from this.

5 VELOCITY VARIATIONS

The positions of the Balmer lines on the detector, as derived by the cross-correlations described in Section 3, appear to show modulation on time-scales similar to those shown by the light curve (see Fig. 2a). This modulation might reflect apparent variations in the line-of-sight velocity of G 29-38. In order to study this in more detail, we determined Doppler shifts for all the spectra by fitting the Hβ, Hγ and Hδ lines (details in Section 5.2 below). The resulting line-of-sight velocity curve is shown in Fig. 2c (upper curve). The Fourier spectrum, shown in Fig. 3b, shows one strong peak, at a frequency of $1634 \pm 5\,\mu$Hz, i.e., consistent with that of the strongest periodicity in the light curve.

Inspired by the close correspondence between the frequencies of these signals, we looked for power at frequencies corresponding to the other ten periodicities in the light curve and found small peaks at some but not all of them (Fig. 3). We determined their amplitudes and phases by fitting the velocity curve with a combination of eleven cosine

waves with frequencies fixed at those determined from the light curve (plus a third-order polynomial to account for slow variations). The results are listed in Table 1 and indicated in Fig. 3b; the residuals are shown in Fig. 2c (bottom curve). Note that unlike for the light curve, the fit to the line-of-sight velocities is formally acceptable ($\chi^2_{\rm red} \simeq 1$) and we expect our error estimates to be reliable.

Could these line-of-sight velocity variations reflect pulsational motion? The pulsations are g-modes and the associated motion is largely horizontal (e.g., Dziembowski 1977). The observed line-of-sight velocity, i.e., the physical velocities projected on the light of sight and integrated over the stellar disk, will thus be dominated by motion near the limb. The observed amplitude will be smaller than the physical velocity amplitude by an amount depending on the spherical degree ℓ and the direction of the pulsation axis relative to the observer. Robinson et al. (1982) estimated the expected line-of-sight velocity amplitudes for typical pulsation amplitudes and found that they should be a few $\mathrm{km\,s^{-1}}$. This is comparable to the amplitudes we find.

If we suppose that the line-of-sight velocity variations reflect horizontal motion associated with the white dwarf pulsation, it is very interesting that all five apparently significant detections ($\geq 2\sigma$) are for periodicities we identified as real modes above; no significant detections are found for the combination frequencies. Before we turn to the implications, however, we need to verify that our error estimates are reasonable and the velocity detections significant; and if so, whether the inferred line-of-sight velocities reflect intrinsic velocity variations rather than some systematic effect in our measurement procedure. We will address these two points in turn.

5.1 Significance of the detections

Looking at Fig. 3b, all peaks but that associated with F1 look insignificant. Indeed, they would be formally insignificant if one did not know the frequency at which to look in advance. However, the pulsation frequencies are determined accurately from the light curve. In the absence of systematic effects (considered separately in Section 5.2), a rough estimate for the significance of a peak with a certain amplitude at a frequency specified in advance can be made by counting the number of other peaks in the velocity spectrum at or above that amplitude. For instance, there are 13 peaks with amplitudes above $2\,\mathrm{km\,s^{-1}}$ at frequencies below 7 mHz (Fig. 3b). With a frequency resolution of $\sim 64\,\mu$Hz, the total number of independent frequency elements in this frequency range is 109, and thus the probability of finding a $\geq 2\,\mathrm{km\,s^{-1}}$ peak by chance at a given frequency is roughly 1:8. One would estimate 1:14 if one counts peaks up to the Nyquist frequency (21 mHz; 23 peaks over $2\,\mathrm{km\,s^{-1}}$ in 322 $[N_{\rm data}/2]$ frequency elements). Thus, F2, F3 and F4, all of which have amplitudes in excess of $2\,\mathrm{km\,s^{-1}}$, are likely real. There is no other peak as large as F1, hence the probability that it is a chance coincidence is $<1:322$.

In order to obtain more quantitative estimates, we ran Monte-Carlo simulations, in which we fitted scrambled velocity curves in the same way as we fitted the observations. The scrambled curves were created by first taking out the slow third-order variation in the measured Doppler shifts, and then re-distributing the resulting velocities randomly over the measurement times. By counting the number of artificial data sets for which the fit produces an amplitude larger than that observed, one can infer the likelihood of a false detection. The likelihood distributions for all periodicities but F3−F1 are consistent with each other (because of its long period, F3−F1 is covariant with the third-order polynomial, and its likelihood distribution is wider). In Fig. 4, we show the cumulative distribution of the amplitudes for all modes but F3−F1 derived from one thousand simulations. We also indicate the observed amplitudes. We infer that F1, F2, F3 and F4 are detected at the >99.9, 98, 98 and 95% confidence levels, respectively; F5 is marginally detected ($\sim$88% confidence); and the signals at all other periodicities are not significant.

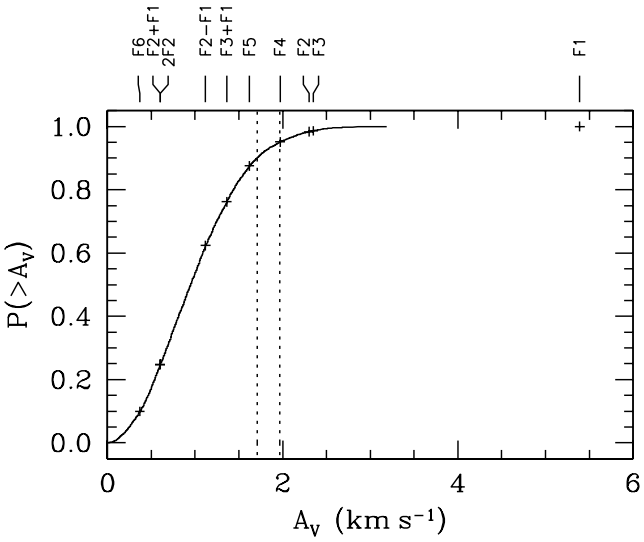

Figure 4. Cumulative distribution of line-of-sight velocity amplitudes derived from simulations with scrambled data. The two dotted lines indicate the amplitudes at which a measurement at a frequency specified in advance has a 90 or 95% probability of being real (i.e., not due to chance). The crosses indicate the amplitudes derived from the fit to the observed line-of-sight velocity curve (Fig. 2). One sees that the detections of real modes F1, F2, F3 and F4 are significant (95% confidence), that of F5 is marginal, and that of F6 is not significant. No significant signal is measured for any of the combination frequencies (F3−F1 is not shown, because its probability distribution is different; see text).

As mentioned above, the fit to the line-of-sight velocities is formally acceptable ($\chi^2_{\rm red} \simeq 1$). The errors, dominated by the star wandering around in the slit (Section 3), should be more or less normally distributed, and thus our error estimates likely reasonable. Indeed, from the simulations one infers similar numbers: $\sigma_A = [\frac{1}{2}\langle A^2\rangle]^{1/2} \simeq 0.8\,\mathrm{km\,s^{-1}}$ (where the factor $\frac{1}{2}$ accounts for the random phase), and $\sigma_\Phi = (180/\pi)(0.8\,\mathrm{km\,s^{-1}}/A_{\rm V})\,\mathrm{deg}$. The exception is F3−F1, for which $\sigma_A = 1.5\,\mathrm{km\,s^{-1}}$, indicating that the uncertainty for this periodicity is underestimated in the least-squares fit (Table 1). This reflects the large covariance with the third-order polynomial.

While the error estimates should be reliable, we caution that the uncertainty distributions are not expected to be normal. This is a consequence of our choice of parameters $A_{\rm V}$ and $\Phi_{\rm V}$. For instance, from Table 1, the uncertainty on

Φ_V is 28 for F5. The 2σ uncertainty, however, is far larger than 56: indeed, at 95% confidence Φ_V can have any value, as the detection of velocity variations at F5 is significant at $< 95\%$ confidence. The uncertainties on $A_V \cos\Phi_V$ and $A_V \sin\Phi_V$ are normally distributed, and one can use these to determine reliable uncertainty estimates for A_V and Φ_V at different confidence levels. Note that the same holds for A_L and Φ_L, but the more significant detections make this less of an issue.

5.2 Possible systematic effects

Above, we have shown that at frequencies at which the flux of the star varies strongly, significant variations are also present in the line-of-sight velocity curve. The question that remains is whether these variations reflect the intrinsic motion in the white dwarf's outer layers expected from the estimates of Robinson et al. (1982), or whether they might be biased or perhaps even result from inadequacies in the way we determined the velocities. For instance, through changes in continuum slope, the measured Doppler shift might be influenced by the variations in temperature with pulsation phase.

For any systematic effect related to the flux variations, the line-of-sight velocity variations have to be either in phase or in anti-phase with the light variations, i.e., the phase difference between velocity and light $\Delta\Phi_V = \Phi_V - \Phi_L = 0$ or 180 deg. This is not what we observe: for F1, $\Delta\Phi_V = 52 \pm 8$ deg. Thus, no more than $A_V \cos\Delta\Phi_V = 3.3\,\mathrm{km\,s^{-1}}$ could be related to systematic effects of this kind. The component out of phase with the light variations has an amplitude of $A_V \sin\Delta\Phi_V = 4.2\,\mathrm{km\,s^{-1}}$, which we can be confident is real given the results of the Monte-Carlo simulations (Fig. 4).

While the above shows that at least part of the line-of-sight velocity signals are intrinsic to the star, the component of the variation that is in phase or anti-phase with the light variations may still be influenced. In order to get a handle on the importance of possible systematics, we tried different methods to determine the line-of-sight velocities, looked at differences between the velocities inferred for different lines, and tried fitting artificial data generated with the models described in Paper II.

We found that cross-correlation was very susceptible to systematics. For instance, the line-of-sight velocity amplitudes derived from the cross-correlation discussed in Section 3 (Fig. 2a) are systematically different for different Balmer lines, both in phase and in amplitude. Most likely, this reflects the influence of the varying temperature and hence continuum slope, which is not accounted for in the cross-correlation procedure. To get unbiased velocities, one needs to normalize all spectra, but it is not clear how to do this properly.

We therefore focused on line-profile fitting, of Hβ, Hγ and Hδ (in the wavelength intervals 4622–5102, 4220–4540 and 4040–4200 Å, respectively). To each line, we fitted a sum of a Lorentzian and a Gaussian profile, with their central wavelengths forced to be the same, and a continuum represented by either a linear or a parabolic function. We tried fitting to $\log F$ in addition to fitting to F directly, the rationale being that since absorption is a multiplicative rather than an additive process, a sum of components can represent $\log F$ better than F.

For all types of fits, the resulting line-of-sight velocity curves were fitted with the combination of eleven cosine waves. The results were systematically different from those inferred from the cross-correlation velocities, with amplitudes generally being somewhat smaller, and phase differences between light and velocity being further away from zero. The systematic differences between lines were smaller, but not absent. No apparent effects are present in the derived phases for the different periodicities, but the amplitudes increase systematically from Hβ to Hγ to Hδ. Also, the zero points (i.e., systemic velocities) derived for the different lines are very different. This is probably unrelated, however, as we find similar differences in systemic velocity for our flux standard G 191B2B, which has much narrower lines. Instead, it likely reflects problems with the wavelength calibration, possibly related to the way the light of the arc lamp is projected on the slit (T. Bida, 1997, private communication). Such an effect should not affect the results for the periodic variations in velocity.

This leaves the systematic differences in the amplitudes found for the individual Balmer lines. We can discard the possibility that these are intrinsic to the star based on a simple analytic derivation: while the intrinsic velocity and light variations are not independent, their dependency is only a second-order effect and hence very small (Paper II). Most likely, therefore, the observed systematic effects in amplitude are still related to our way of fitting, perhaps simply because our choice of Lorentzian plus Gaussian is an inadequate model for the observed line profiles.

To get a better handle on the problem, we fitted a number of artificial data sets, produced using the procedures described in Paper II, for different settings of temperature amplitude, horizontal surface velocity amplitude, phase difference between light and velocity, and spherical degree[‡].

For all artificial data sets and fitting methods, the results for the different lines showed systematic differences of comparable magnitude to those seen in the real data. A set with zero input temperature variation gave the same velocity amplitude and phase for all three lines, as should be the case, but different systemic velocity, with Hγ being close to zero, and Hβ and Hδ being negative and positive, respectively, by an amount that depended on the fitting method. The amount was smaller for fitting $\log F$ than for fitting F directly, as expected (-13, -1, $+11\,\mathrm{km\,s^{-1}}$ for Hβ, Hγ, Hδ, respectively).

For data sets with non-zero temperature variations, Hγ again reproduced the input values best, in the sense that the systemic value was still closest to zero, and the velocity phase delay closest to the input value. Hβ and Hδ tended to lower and higher amplitude and to larger and smaller phase delay, respectively, with the values for both amplitude and phase being more or less symmetric around those for Hγ. From a set with no velocity variations put in, we find that for a temperature variation corresponding to 2.8% modula-

‡ In principle, we could have tried fitting the models directly to the observations. We decided not to do this both because the models do not reproduce the observed variations all that well, and because it would make verifying our results much more difficult.

tion at 5500 Å, the apparent velocity shifts in Hβ and Hδ are about $0.6\,\mathrm{km\,s^{-1}}$ in amplitude. The systematic differences with Hγ for sets including velocity variations are consistent with this. The amplitude should be compared with the observed radial velocity amplitude of $\sim 3\,\mathrm{km\,s^{-1}}$ and the uncertainty of $0.8\,\mathrm{km\,s^{-1}}$.

Given the results on the artificial data and taking into account that the observed velocity signals have low signal-to-noise, we decided to use the average of the Hβ, Hγ and Hδ velocities, determined by fitting to $\log F$ (with a linear slope for the continuum). The resulting line-of-sight velocity curve is the one discussed above and shown in Fig. 2c. It has uncertainties dominated by the effects of the star wandering around in the slit. Given the simulations with the artificial data, we feel reasonably confident that systematic effects in the fitted amplitudes and phases will be smaller than the quoted uncertainties derived from the least-squares fit (as listed in Table 1). For completeness, we note that the result would be similar if one were to use the velocities derived from Hγ only.

5.3 Velocity summary

We conclude that we have detected line-of-sight velocity variations which are due to intrinsic processes in the white dwarf, and which have amplitudes comparable with those expected from the integration over the visible disk of the surface motion due to the pulsations (Robinson et al. 1982). We have shown that our estimates of the uncertainties are robust and that systematic effects, while problematic, most likely will be within these uncertainties. Out of the eleven strongest modes present in the light curve, five out of six of the real modes show significant modulation, while none of the combination frequencies does, even though F2+F1 and 2F2 have light amplitudes similar to those of the weaker real modes F4 and F5.

6 DISCUSSION

In this section, we discuss the observational results for the real modes and the combination frequencies in some detail. For each group, we describe the general properties we regard as important, mention what can be understood from geometrical arguments alone, and discuss the results in the context of convective-driving models.

6.1 Real modes

We mentioned already that only the real modes show significant modulation in the line-of-sight velocities. As measures of the relative amplitudes and phases of velocity and light, we use $R_\mathrm{V} = (A_\mathrm{V}/2\pi f)/A_\mathrm{L}$ and $\Delta\Phi_\mathrm{V} = \Phi_\mathrm{V} - \Phi_\mathrm{L}$ (see Table 1). Here, A_V and A_L are the observed line-of-sight velocity and fractional light amplitudes, Φ_V and Φ_L the corresponding phases, and f the frequency of the mode. The ratio R_V does not depend on azimuthal order m and aspect (see Dziembowski 1977; Paper II). The rationale for including f is that with this definition R_V depends only on spherical degree ℓ for adiabatic pulsations. For adiabatic pulsations, one also has $\Delta\Phi_\mathrm{V} = 90$, i.e., velocity maximum arrives a quarter cycle after light maximum.

From Table 1, we see that the values of both R_V and $\Delta\Phi_\mathrm{V}$ show no significant variation among the different real modes. All values of $\Delta\Phi_\mathrm{V}$ are between 0 and 90, i.e., velocity lags light, but by less than a quarter cycle.

The largest value of R_V is found for mode F4. While the difference with the values for the other modes is not formally significant, we note that a larger value is consistent with this mode having $\ell = 2$ and the others $\ell = 1$, as inferred in Paper II from the wavelength dependences of the pulsation amplitudes. Compared to an $\ell = 1$ mode, the light variations for an $\ell = 2$ mode are subject to stronger cancellation, while the surface velocities are actually easier to observe (see Dziembowski 1977).

In the interior of a white dwarf, pulsation associated with a real mode should be largely adiabatic; maximum flux coincides with maximum compression and is followed a quarter cycle later by matter moving away at maximum velocity. This will change as the mode propagates upward and enters the outer regions, where non-adiabatic effects become important. Using the observed relations between light and line-of-sight velocity variations, we can therefore hope to infer properties of the surface layers.

In the convective-driving picture (Brickhill 1992a; Goldreich & Wu 1999a), the main source of change is the surface convection zone. As this region bottles up heat when it is heated, the flux perturbations at the photosphere of the star are diminished in magnitude and delayed in phase compared to those entering the bottom of the convection zone. In contrast, the horizontal velocities associated with the pulsation are nearly independent of depth inside the convection zone, because of the strong turbulent viscosity (Brickhill 1990; Goldreich & Wu 1999b). Thus, values of R_V should be larger than those expected for adiabatic pulsations, and values of $\Delta\Phi_\mathrm{V}$ smaller than 90.

The effects are expected to become more prominent with increasing values of $\omega\tau_C$, where $\omega \equiv 2\pi f$ is the angular frequency of the mode and τ_C is the so-called thermal adjustment time (Goldreich & Wu 1999a; quantity D in Brickhill 1983), which is a few times the thermal time at the bottom of the convection zone. With increasing mode frequency, therefore, R_V should increase and $\Delta\Phi_\mathrm{V}$ should deviate more and more from 90, tending towards 0.

Indeed, the observed values of $\Delta\Phi_\mathrm{V}$ are smaller than 90 and those for R_V larger by a factor 2–3 than expected if one were to neglect non-adiabatic effects (e.g., $R_{\mathrm{V,ad}} \simeq 6$ for mode F1). Unfortunately, the observations do not allow one to verify the predicted trends, but it may be worth noting that, if anything, $\Delta\Phi_\mathrm{V}$ shows a trend opposite to that predicted, i.e., less of a deviation from 90 for shorter periods. We remind the reader that the errors in $\Delta\Phi_\mathrm{V}$ are not distributed normally (Section 5.1).

It is difficult to make a more quantitative comparison, as this requires evaluating the thermal adjustment time τ_C, which depends on details of the convection. Ideally, one would like to use R_V and $\Delta\Phi_\mathrm{V}$ to estimate τ_C and thus constrain the convection properties. Our data only allow a rough determination: a 800-s mode in a star with $\tau_C = 300\,\mathrm{s}$ has $R_\mathrm{V} \simeq 16$ and $\Delta\Phi_\mathrm{V} \simeq 50$ (Wu & Goldreich 1998), similar to what is observed for mode F2.

An independent constraint to τ_C can be inferred from the longest-period mode that is present. This is because to excite a gravity-mode, the convection zone needs to extend

deep enough for its thermal response time to be of order of or longer than the mode period, i.e., $\omega\tau_C > 1$ (Brickhill 1983; Goldreich & Wu 1999a). The longest-period mode is F2 at 818 s (or F7 at 1106 s; see Appendix), and thus τ_C130 s (180 s), consistent with the above value. Consistent estimates of τ_C are also obtained using combination frequencies (see below).

6.2 Combination frequencies

The lack of line-of-sight velocity signals at the frequencies which we associate with combinations of real modes, confirms the notion that combination frequencies do not reflect physical pulsation, but rather mixing of the parent-mode signals by a non-linear transformation occurring in the outer layers of the white dwarf.

We quantify the combination frequencies using an amplitude ratio $R_{\rm C} = A_{\rm L}^{i\pm j}/n_{ij}A_{\rm L}^{i}A_{\rm L}^{j}$ and a phase difference $\Delta\Phi_{\rm C} = \Phi_{\rm L}^{i\pm j} - (\Phi_{\rm L}^{i} \pm \Phi_{\rm L}^{j})$. Here, $A_{\rm L}^{i\pm j}$ and $\Phi_{\rm L}^{i\pm j}$ are the observed amplitude and phase of a combination at frequency $f^i \pm f^j$ of real modes i and j (with frequencies f^i and f^j, amplitudes $A_{\rm L}^{i}$ and $A_{\rm L}^{j}$, and phases $\Phi_{\rm L}^{i}$ and $\Phi_{\rm L}^{j}$); n_{ij} is the number of possible permutations: $n_{ij} = 1$ for $i = j$ and $n_{ij} = 2$ for $i \neq j$; i and j are chosen such that difference frequencies are positive. We include n_{ij} to ensure that the harmonic of a single mode and a combination of two modes with almost identical properties would lead to the same $R_{\rm C}$ (cf. Brickhill 1992b). Similar definitions are used for the 3-mode combinations (see Table A1); below, we focus on combinations of two modes.

The observed values of $R_{\rm C}$ and $\Delta\Phi_{\rm C}$ (Tables 1 and A1) vary significantly from mode to mode, although part of the variation is due to only a few outliers (especially 2F4, which we will discuss in more detail below). There appears to be some correlation between the value of $R_{\rm C}$ and the amplitudes of the parent modes, with $R_{\rm C}$ increasing for decreasing $A_{\rm L}^{i,j}$. The phase differences $\Delta\Phi_{\rm C}$ cluster around zero (within ~ 45); this reflects the sharp maxima and shallow minima in the light curve.

If the combination frequencies indeed result from nonlinear mixing in the upper layers of the star, then independent of a specific theory one expects a combination frequency to have at any point on the surface a flux amplitude proportional to the product of its parent-mode amplitudes at that point. The surface distributions of the parent modes are described by spherical harmonics. Therefore, the surface distribution of the combination frequency will be proportional to the product of spherical harmonics, which can in turn be described by a linear superposition of spherical harmonics with different ℓ (see, e.g., Abramowitz & Stegun 1972; we adopt their notation).

In the following discussion, we will assume all parent modes have only $m = 0$ components. We consider the more general case later. First, we study the first harmonic of a single parent mode. The first harmonic of a parent mode with $(\ell, m) = (1, 0)$ has a surface distribution described by $Y_1^0 Y_1^0$, which can be decomposed into a sum of Y_0^0 and Y_2^0 distributions. The first harmonic of a parent mode with $(\ell, m) = (2, 0)$ has a surface distribution that is the sum of three components, Y_0^0, Y_2^0 and Y_4^0. The numerical factors in front of the Y_0^0 terms are the same for both decompositions. When integrated over the visible hemisphere, the (2,0) parent mode will suffer stronger cancellation than the (1,0) parent mode. On the other hand, their harmonics will typically be dominated by Y_0^0 components that do not suffer from cancellation. Therefore, $R_{\rm C}$ will be higher for the harmonic of the (2,0) mode. This conclusion is independent of the the angle between the line-of-sight and the pulsation axis.

In Table A1, the value of $R_{\rm C}$ for 2F4 is much larger than, e.g., that for 2F1 and 2F2. While we should caution that 2F4 could be blended with other combinations, this is exactly what one would expect from the example given above, given our identifications of F1 and F2 with $\ell = 1$ and F4 with $\ell = 2$ (Paper II). Note that one would not expect, e.g., F4+F1 to have a value of $R_{\rm C}$ larger than those for combinations of two $\ell = 1$ modes, such as F2+F1, F3+F1 and F5+F1 (as observed; Table A1). This is because the product $Y_2^0 Y_1^0$ has no Y_0^0 component and therefore suffers cancellation.

Looking in detail at $R_{\rm C}$ for all combinations involving F1 and another $\ell = 1$ mode, e.g., 2F1, F2+F1, we find that the values are not consistent with being the same. There appears to be a trend of increasing $R_{\rm C}$ with decreasing parent-mode amplitude. A similar trend appears to be present for the 3-mode combination frequencies. This is not expected, as generally the efficiency of mixing should be relatively independent of the amplitudes of the input signals when these signals are weak.

We should caution that above we have been neglecting the possible effect of different values of m. For instance, the harmonic of a $\ell = 1$, $m \neq 0$ parent mode is described by a Y_2^{2m} distribution only; it would have a low value of $R_{\rm C}$. In our short observations, we cannot resolve the rotation-induced frequency splitting among different m components that has been seen previously for some of the modes (Kleinman et al. 1998). Thus, the power at both the harmonic and its parent mode may result from a number of combinations, which makes our conclusions uncertain. They can likely be verified, however, using existing, much longer time series from WET.

We now turn from these general considerations, valid for any local nonlinear mixing scheme, to a comparison of our data with numerical results and analytic calculations based on the convective-driving mechanism. As mentioned, in this picture flux perturbations appearing at the photosphere are diminished and delayed relative to those that enter the convection zone, by an amount that depends on the depth of the convection zone (and thus τ_C). The depth of the convection zone, however, depends sensitively on the photospheric temperature. The latter varies due to the pulsations, and, therefore, the depth of the convection will vary as well. The associated variation in reduction and delay leads to a distortion of the pulsation signal at the photosphere, which translates into the power seen at the combination frequencies (Brickhill 1992b; Wu 1997).

Brickhill (1992b) found that $R_{\rm C}$ will be 6 for the first harmonic of an $(\ell, m) = (1, 0)$ mode and 16 for that of a (2,0) mode, the exact values depending on the frequencies, τ_C and the angle between the line of sight and the pulsation axis. He found sum frequencies share similar values of $R_{\rm C}$ with

the harmonics[§], while difference frequencies from the same pair of parent modes have lower values. These results were confirmed analytically by Wu (1997), who found that for combinations with relatively high frequency ($(\omega^{i\pm j}\tau_C \gg 1$), R_C should be approximately constant and $\Delta\Phi_C$ approximately zero, while towards lower frequencies ($\omega^{i\pm j}\tau_C \simeq 1$), R_C should be lower and $\Delta\Phi_C$ should shift towards -90 .

The observed values of R_C and $\Delta\Phi_C$ compare, on average, favourably to the expectations. The typical values of R_C are reproduced with $\tau_C \simeq 200\,\mathrm{s}$ (Wu 1997), which is consistent with the values of τ_C inferred above from the longest-period overstable mode and the velocity-light comparison (Section 6.1).

Little evidence is found for the expected trends of either R_C or $\Delta\Phi_C$ with frequency of the combinations. In part, this might be due to our inability to resolve components of different m. Again, it would be good to verify these conclusions with longer time series, such as those already available from WET.

As mentioned, a trend of R_C with parent-mode amplitude is not expected in any simple non-linear mixing theory (e.g., Wu 1997). Nevertheless, the numerical calculations presented by Brickhill (1992b) show an amplitude dependence of R_C for 3-mode combinations that is similar to that observed (and with similar numerical values). At present, we do not understand why this dependence arises in the simulations; unfortunately, Brickhill does not expand on it.

7 CONCLUSIONS

We have applied the tool of time-resolved spectrophotometry to the study of pulsating white dwarfs. In this paper, we showed that at our very high signal-to-noise ratios we can detect the small line-of-sight velocity variations associated with the g-mode pulsations, at amplitudes similar to those expected (Robinson et al. 1982). Significant velocity variation is seen for five out of the six modes we believed were real. For all five modes, the phase difference $\Delta\Phi_V$ between velocity and light is between 0 and 90, i.e., velocity maximum occurs later than flux maximum, but by less than the quarter cycle expected for adiabatic pulsations. The amplitude ratios R_V are similar for the five modes. The largest value occurs for mode F4 (at 776 s), which is consistent with mode F4 having $\ell = 2$ and the others $\ell = 1$, as was inferred from the wavelength dependence of the pulsation amplitudes in Paper II.

No significant line-of-sight velocity variation is seen for any of the five combination frequencies, even though two of these have light amplitudes comparable to that of the fourth strongest real mode. This provides independent confirmation that the combination frequencies do not reflect physical pulsation. Rather, they likely result from mixing of mode power by a non-linear transformation in the outer layers of the star. The phase differences $\Delta\Phi_C$ between combination frequencies and parent modes are all close to zero, reflecting the sharp maxima and shallow minima in the light curve. The amplitude ratios R_C show significant differences, but are generally within a factor two of each other. The exception is the four times larger value for the harmonic of mode F4. This difference is again consistent with the differences in ℓ between mode F4 and the others.

Models for the interaction between pulsation and convection can broadly reproduce the observed values of R_V and $\Delta\Phi_V$ for the real modes, as well as those of R_C and $\Delta\Phi_C$ for the combination frequencies (Brickhill 1992b; Wu 1997). The models are internally consistent, in that the inferred thermal properties of the convection zone are such that modes at the observed periods are expected to be overstable. In detail, there are some problems, with $\Delta\Phi_V$ showing a trend with frequency opposite of that expected, and the mixing strength, reflected in R_C, not showing the expected correlation with frequency, but rather a possible dependency on parent-mode amplitude. Both these need confirmation; for the former, further time-resolved spectroscopy is needed, but for the latter, excellent data already exist. We also hope that our results will lead to further theoretical efforts.

In summary, time-resolved spectroscopy offers insight in the white dwarf interiors at three levels. By measuring the effects of temperature variation at different wavelengths, the temperature structure of the atmosphere can be calibrated. Using the velocity changes and the combination frequencies, one can constrain the convection zone below the photosphere. And finally, with the determination of the spherical degree and hence the more secure identifications of periodicities with eigen-modes, one can use asteroseismology to probe the interior with greater confidence.

Acknowledgments

We gratefully acknowledge help of Wayne Wack with the observations, useful discussions with Tom Bida about intricacies of LRIS and with Peter Goldreich, Scot Kleinman and Rob Robinson about white-dwarf pulsations, as well as sceptical and therefore very useful remarks by an anonymous referee. M.H.v.K. acknowledges a NASA Hubble Fellowship while at Caltech, and a fellowship of the Royal Netherlands Academy of Arts and Sciences at Utrecht. This research has made use of the Simbad database, operated at CDS, Strasbourg, France. The observations were obtained at the W. M. Keck Observatory, which is operated by the California Association for Research in Astronomy, a scientific partnership among the California Institute of Technology, the University of California, and the National Aeronautics and Space Administration. It was made possible by the generous financial support of the W. M. Keck foundation. The reduction was done within the environment of the Munich Image Data Analysis System, which is developed and maintained by the European Southern Observatory.

REFERENCES

Abramowitz M. & Stegun I. A. (eds) 1972, Handbook of Mathematical Functions (New York: Dover)

Beland S., Boulade O., Davidge T., 1988, CFHT Info. Bull., 19, 16

Bergeron P., Wesemael F., Lamontagne R., Fontaine G., Saffer R. A., Allard N. F., 1995, ApJ, 449, 258

Bohlin R. C., Colina L., Finley D. S., 1995, AJ, 110, 1316

§ Brickhill (1992b) discusses but does not correct for the number of permutations n_{ij}.

Brickhill A. J., 1983, MNRAS, 204, 537
Brickhill A. J., 1990, MNRAS, 246, 510
Brickhill A. J., 1991a, MNRAS, 251, 673
Brickhill A. J., 1991b, MNRAS, 252, 334
Brickhill A. J., 1992a, MNRAS, 259, 519
Brickhill A. J., 1992b, MNRAS, 259, 529
Clemens J. C., 1993, Baltic Astr., 2, 407
Clemens J. C., van Kerkwijk M. H., Wu Y., 1998, MNRAS, submitted (Paper II)
Dziembowski W., 1977, Acta Astr., 27, 203
Goldreich P., Wu Y., 1999a, ApJ, 511, 904
Goldreich P., Wu Y., 1999b, ApJ, submitted (astro-ph/9810038)
Horne K., 1986, PASP, 98, 609
Kawaler S. D., Bradley P. A., 1994, ApJ, 427, 415
Kleinman S. J., 1995, PhD thesis, University of Texas at Austin
Kleinman S. J., et al., 1994, ApJ, 436, 875
Kleinman S. J., et al., 1998, ApJ, 495, 424
Koester D., Provencal J., Shipman H. L., 1997, A&A, 230, L57
McCook G. P., Sion E. M., 1987, ApJS, 65, 603
McGraw J. T., Robinson E. L., 1975, ApJ, 200, l89
Nather R. E., Winget D. E., Clemens J. C., Hansen C. J., Hine B. P., 1990, ApJ, 361, 309
Oke J. B., et al., 1995, PASP, 107, 375
Robinson E. L., Kepler S. O., Nather R. E., 1982, ApJ, 259, 219
Robinson E. L., et al., 1995, ApJ, 438, 908
Shulov O. S., Kopatskaya E. N., 1974, Astrofizika, 10, 117
Winget D. E., et al., 1990, ApJ, 357, 630
Winget D. E., et al., 1991, ApJ, 378, 326
Winget D. E., et al., 1994, ApJ, 430, 839
Wu Y., 1997, PhD thesis, California Institute of Technology
Wu Y., Goldreich P., 1999, ApJ, accepted (astro-ph/9812085)
Young A. T., 1967, AJ, 72, 747
Zuckerman B., Becklin E. E., 1987, Nature, 330, 138

APPENDIX A1: FURTHER PERIODICITIES

The light curve we obtained is not described well by variations at the eleven frequencies we identified in Section 4. In particular, there are a quite a few more peaks present in the Fourier transform at combination frequencies. We have continued the identification process until no peaks with amplitudes larger than 0.3% remained. This gave us 29 frequencies¶. At this point, the Fourier spectrum of the residuals became too noisy to identify with any confidence more peaks in the main region of power (1–4 mHz). In the cleaner region at higher frequencies, however, there were still four peaks coincident with frequencies expected for 3-mode combinations. Since these might be of particular interest for modeling the pulsations, we included these in a final fit. The frequencies, amplitudes and phases for all 33 periodicities are listed in Table A1, and indicated in Fig. A1a. We also fitted the velocities to this set of 33 periodicities. The results are indicated in Fig. A1b; calculated values of $R_{\rm V}$ and $\Delta\Phi_{\rm V}$ for the real modes are listed in Table A1.

We conclude with a few remarks. First, we note that possible significant periodicity is also present for 2F3 ($A_{\rm L} = 0.21 \pm 0.05\%$, $\Phi_{\rm L} = -3 \pm 14$, $R_{\rm C} = 9.7 \pm 2.4$, $\Delta\Phi_{\rm C} = -83 \pm 14$) and F5+F2 ($0.12 \pm 0.05\%$, -117 ± 26, 4.0 ± 1.9, 62 ± 26), while no significant signal is seen at 2F5 ($0.05 \pm 0.05\%$, $R_{\rm C} = 17 \pm 17$). One might have expected power at a number of combination frequencies not present in Table A1, such as F3−F2 and F7±F1. These may indeed be present, but their frequencies are so close to other combinations that it is impossible to include them in the fit. Which of the possible combinations one uses is a matter of choice. We have been biased by theory in preferring those for which the parent modes have larger amplitudes, or, if similar, those for which the fitted value of $\Delta\Phi_{\rm C}$ was closest to 0.

Second, the periodicity F9, which is very close to F1 in period, is rather uncertain. The modulation could be fitted equally well with a variable amplitude for F1. If F9 is real, it should have $\ell \neq 1$ given its proximity to F1, which has $\ell = 1$. If it has $\ell = 2$ and a substantial $m = 0$ component, one might expect a large harmonic, like for F4. This harmonic might in part account for the peak now described by F9+F1; if we fit 2F9 instead (we cannot fit both jointly), we find $A_{\rm L} = 0.26 \pm 0.05\%$, $\Phi_{\rm L} = 109 \pm 12$, which corresponds to $R_{\rm C} = 36 \pm 17$, similar to that of 2F4, but $\Delta\Phi_{\rm C} = -160 \pm 20$, much

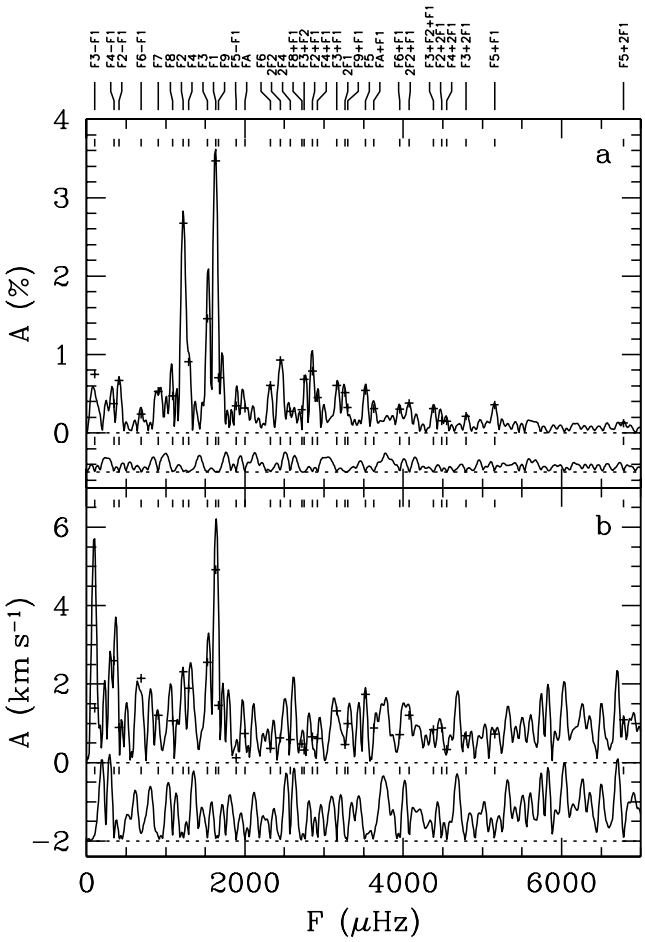

Figure A1. Fourier transform of the light curve (a) and line-of-sight velocity curve (b), with 33 identified peaks indicated and labeled. The pluses indicate the amplitudes derived from fitting cosine waves (plus a constant for the light curve and a cubic polynomial for the line-of-sight velocity curve). The bottom curve in each panel shows the Fourier transform of the residuals, offset from zero for clarity.

¶ The fitted amplitude is not always larger than 0.3% for combination frequencies, as for these the frequency is fixed at the sum or difference of the frequencies of the parent modes, which may not lead to a complete removal of the peak in the Fourier transform.

further removed from zero than for any other combination frequency.

Finally, while for most combination frequencies we do not find significant velocity variation, there are two exceptions: F4−F1 at 2900 s and F6−F1 at 1447 s. These two periodicities appear harmonically related to each other, and we believe the associated velocity signals reflect either instrumental or atmospheric effects rather than physical variations. We briefly wondered about possible orbital modulation, but observations at higher resolution did not confirm these periodicities.

Table A1. Pulsation Frequencies in G 29-38

Real mode	P (s)	f (μHz)	$A_{\rm L}$ (%)	$\Phi_{\rm L}$ ()	$A_{\rm V}$ (km s^{-1})	$\Phi_{\rm V}$ ()	$R_{\rm V}$	$\Delta\Phi_{\rm V}$ ()
F1	613	1631.5 ± 0.9	$3.47 \pm .14$	-174 ± 2	4.9 ± 1.0	-122 ± 12	14 ± 3	52 ± 12
F2	818	1222.4 ± 0.6	$2.67 \pm .05$	132 ± 1	2.3 ± 0.8	177 ± 19	11 ± 4	45 ± 19
F3	655	1527.5 ± 1.1	$1.46 \pm .05$	40 ± 2	2.6 ± 0.8	61 ± 18	19 ± 6	21 ± 18
F4	777	1286.7 ± 1.7	$0.91 \pm .05$	44 ± 4	1.9 ± 0.8	53 ± 23	26 ± 11	9 ± 23
F5	284	3521.5 ± 2.5	$0.54 \pm .05$	50 ± 5	1.7 ± 0.8	132 ± 25	14 ± 7	82 ± 25
F6	431	2322.5 ± 2.6	$0.61 \pm .05$	-85 ± 5	0.4 ± 0.8	···	4 ± 9	···
F7	1106	903.9 ± 3.4	$0.53 \pm .05$	-125 ± 5	1.2 ± 0.8	···	40 ± 27	···
F8	920	1086.7 ± 3.9	$0.47 \pm .05$	141 ± 6	1.1 ± 0.8	···	34 ± 25	···
F9	601	1664.9 ± 6.0	$0.71 \pm .14$	-43 ± 8	1.5 ± 1.0	···	20 ± 14	···
FA	500	1998.4 ± 4.2	$0.32 \pm .05$	77 ± 9	0.7 ± 0.8	···	17 ± 20	···
2-mode combination	P (s)	f (μHz)	$A_{\rm L}$ (%)	$\Phi_{\rm L}$ ()	$A_{\rm V}$ (km s^{-1})	$\Phi_{\rm V}$ ()	$R_{\rm C}$	$\Delta\Phi_{\rm C}$ ()
2F1	306	3263.0	$0.52 \pm .08$	-10 ± 9	0.5 ± 1.0	···	4.3 ± 0.7	-22 ± 10
F2 + F1	350	2853.9	$0.79 \pm .05$	-35 ± 4	0.7 ± 0.8	···	4.3 ± 0.3	7 ± 5
F2 − F1	2444	409.2	$0.67 \pm .05$	29 ± 4	0.9 ± 0.8	···	3.6 ± 0.3	-25 ± 5
2F2	409	2444.7	$0.93 \pm .05$	-132 ± 3	0.6 ± 0.8	···	13.0 ± 0.9	-37 ± 4
F3 + F1	317	3159.0	$0.61 \pm .05$	-117 ± 5	1.3 ± 0.8	···	6.0 ± 0.6	17 ± 6
F3 − F1	9612	104.0	$0.75 \pm .05$	158 ± 4	1.4 ± 1.3	···	7.4 ± 0.7	11 ± 5
F3 + F2	364	2749.9	$0.69 \pm .08$	147 ± 6	0.3 ± 1.1	···	8.8 ± 1.1	-26 ± 6
F4 + F1	343	2918.2	$0.45 \pm .05$	-155 ± 7	0.6 ± 0.8	···	7.1 ± 0.9	-25 ± 8
F4 − F1	2900	344.9	$0.38 \pm .05$	-163 ± 8	2.6 ± 0.8	-38 ± 17	6.0 ± 0.9	54 ± 9
2F4	389	2573.3	$0.27 \pm .05$	91 ± 10	0.6 ± 0.8	···	33.2 ± 7.1	4 ± 13
F5 + F1	194	5153.1	$0.36 \pm .05$	-127 ± 8	0.7 ± 0.8	···	9.5 ± 1.6	-3 ± 10
F5 − F1	529	1890.0	$0.35 \pm .05$	-129 ± 8	0.1 ± 0.8	···	9.2 ± 1.6	7 ± 10
F6 + F1	253	3954.0	$0.30 \pm .05$	152 ± 9	0.7 ± 0.8	···	7.2 ± 1.3	50 ± 11
F6 − F1	1447	690.9	$0.24 \pm .05$	55 ± 12	2.1 ± 0.8	-130 ± 20	5.7 ± 1.3	-34 ± 13
F8 + F1	368	2718.2	$0.30 \pm .08$	-32 ± 13	0.5 ± 1.0	···	9.1 ± 2.7	1 ± 15
F9 + F1	303	3296.4	$0.32 \pm .08$	114 ± 13	1.0 ± 1.0	···	6.6 ± 2.1	-30 ± 15
FA + F1	275	3629.9	$0.31 \pm .05$	-87 ± 9	0.9 ± 0.8	···	14.0 ± 3.2	9 ± 13
3-mode combination	P (s)	f (μHz)	$A_{\rm L}$ (%)	$\Phi_{\rm L}$ ()	$A_{\rm V}$ (km s^{-1})	$\Phi_{\rm V}$ ()	$R_{\rm C}$	$\Delta\Phi_{\rm C}$ ()
2F2 + F1	245	4076.3	$0.38 \pm .05$	55 ± 8	1.2 ± 0.8	···	51 ± 7	-36 ± 8
F3 + F2 + F1	228	4381.4	$0.31 \pm .05$	-11 ± 9	0.8 ± 0.8	···	39 ± 7	-9 ± 10
F2 + 2F1	223	4485.4	$0.16 \pm .05$	136 ± 18	0.9 ± 0.8	···	16 ± 5	-9 ± 19
F3 + 2F1	209	4790.5	$0.22 \pm .05$	69 ± 13	0.7 ± 0.8	···	41 ± 10	16 ± 14
F4 + 2F1	220	4549.7	$0.15 \pm .05$	18 ± 19	0.3 ± 0.8	···	46 ± 16	-38 ± 20
F5 + 2F1	147	6784.6	$0.13 \pm .05$	78 ± 22	1.1 ± 0.8	···	64 ± 26	15 ± 23

Notes. For the real modes, $R_{\rm V} = (A_{\rm V}/2\pi f)/A_{\rm L}$ in units of 10 km rad^{-1} %$^{-1}$ and $\Delta\Phi_{\rm V} = \Phi_{\rm V} - \Phi_{\rm L}$. For the 2-mode combination frequencies, $f = f^i \pm f^j$, with for difference frequencies i and j chosen such that f is positive, $R_{\rm C} = A_{\rm L}^{i\pm j}/n_{ij}A_{\rm L}^i A_{\rm L}^j$, with n_{ij} the number of possible permutations, and $\Delta\Phi_{\rm C} = \Phi_{\rm L}^{i\pm j} - (\Phi_{\rm L}^i \pm \Phi_{\rm L}^j)$. Similarly, for 3-mode combination frequencies, $f = f^i + f^j + f^k$, $R_{\rm C} = A_{\rm L}^{i+j+k}/n_{ijk}A_{\rm L}^i A_{\rm L}^j A_{\rm L}^k$ and $\Delta\Phi_{\rm C} = \Phi_{\rm L}^{i+j+k} - (\Phi_{\rm L}^i + \Phi_{\rm L}^j + \Phi_{\rm L}^k)$. The uncertainties in the parameters for the light curve should be seen as indicating relative uncertainties only, as the light curve is not described well by the modes fitted and the deviations from the fit are definitely not distributed normally. The estimates given here were obtained by multiplying the observational errors by such a factor that $\chi^2_{\rm red} = 1$. For the velocity curve, the estimates of the uncertainties should be reliable. The uncertainty distributions on amplitude and phase are not normal, but those on $A\cos\Phi$ and $A\sin\Phi$ are (see Section 5.1).